



Adhesion of electrodes on diamond (111) surface: A DFT study

Tom Ichibha^{a,*}, Kenta Hongo^{b,c,d}, I. Motochi^e, N.W. Makau^f, G.O. Amolo^g, Ryo Maezono^b

^a School of Materials Science, JAIST, Asahidai 1-1, Nomi, Ishikawa 923-1292, Japan

^b School of Information Science, JAIST, Asahidai 1-1, Nomi, Ishikawa 923-1292, Japan

^c National Institute of Materials Science, Tsukuba, Ibaraki, Japan

^d PRESTO, JST, Kawaguchi, Saitama, Japan

^e Department of Mathematics and Physical Sciences, Maasai Mara University, Narok, Kenya

^f Computational Materials Science Group, Department of Physics, University of Eldoret, Eldoret, P.O. Box 1125-30100, Kenya

^g Department of Physics and Space Science, The Technical University of Kenya, Nairobi, P.O. Box 52428-00200, Kenya

ARTICLE INFO

Keywords:

Electrodes on diamond device

Surface termination

Power device

ABSTRACT

We explore possible candidates for metallic electrodes of diamond semiconductor from twenty kinds of metallic sheets on oxygen- or hydrogen-terminated diamond (111) surface as well as pristine one. Their adhesion strengths and electric characteristics of contacts (*i.e.* either Ohmic, Schottky or neither) are both considered as figures of merit. The former is measured as work of separation, W_{sep} , obtained from density functional theory (DFT) simulations. The latter is inferred from DOS (density of states) analysis based on DFT, by checking whether or not the in-gap peak disappears and if there is a large DOS around the Fermi level. We found that (1) Ti on pristine surface has both the best Ohmic contact and fairly strong adhesion and (2) Ti and Cr on oxygenated surfaces have the strongest adhesion with good Schottky contact.

1. Introduction

Diamond is a promising candidate for the next-generation power devices, possessing a wider band gap by a factor of five and a higher thermal conductivity by a factor of more than ten [1], compared with Si [2,3]. These properties are key for the device robustness in its anti-voltage and anti-thermal strengths which is required especially in power semiconductor devices. Its higher electron mobility, 1.3 times or more faster than Si, makes the device a very good candidate for use in signal processing with higher frequencies.

Nevertheless, diamond semiconductors have not been widely spread yet in the practical situations. One of the primary reasons is the difficulty of synthesizing big diamond single crystals. Microwave plasma assisted chemical vapor deposition (MPCVD) is often used for the synthesis [4–7], with which inch-size diamond (100) is established [6]. Another issue for diamond device is poor concentration of carriers in pristine diamond. To give large amounts of carrier density especially for power devices, doping techniques are usually employed. Boron has the lowest activation energy for doping, 0.37 eV, so the synthesis of boron doped diamond (BDD), p-type semiconductor, has been eagerly studied [8–12], and high carrier density doping, 10^{20} cm^{-3} , has already been established by applying high pressure [9]. Furthermore, the coexistence of high carrier density and high carrier

mobility is generally not allowed because of the insulator transition of BDD at high carrier density, $5 \times 10^{20} \text{ cm}^{-3}$ [12]. Delta doping technique has recently been reported to be a good solution [11,12].

Phosphorus doping has been applied for diamond (111), where diamond becomes n-type semiconductor, different from boron doping. While high carrier density, 10^{20} cm^{-3} , is established [13,14], the growth of fairly large diamond (100) with good quality is quite challenging today [14]. Thus, phosphorus doping for diamond (100) has been eagerly studied and also fairly high carrier density, around 10^{18} cm^{-3} , is established [15].

Another important issue is electrode fabrication, namely about the establishment of low contact resistance. Refractory metals (*e.g.* Ti, Mo, W, Cr, and Ta) covered by noble metals, Au and Pt, are usually employed for electrodes [16–20]. Refractory metals form carbides after annealing and noble metals prevent the corrosion of refractory metals [17]. Meyyappan et al. annealed Ti-W alloy and Cr both covered by Au. They established the interdiffusion between Au and Ti-W or Cr occurs and confirmed such a tendency is more subdued for Cr [16]. Johnston et al. annealed Ti, Mo, W, and Ta covered by Au or Pt and established Pt significantly prevents the interdiffusion [17]. Iacovangelo and Hoff et al. studied trilayer electrode, Ti/Pt/Au, where Pt works to prevent Ti from penetrating into the Au layer [18,19]. The recent study by Msolli et al. has reported that a trilayer electrode, Ti/

* Corresponding author.

E-mail address: s1720002@jaist.ac.jp (T. Ichibha).

<https://doi.org/10.1016/j.diamond.2017.12.008>

Received 25 August 2017; Received in revised form 5 December 2017; Accepted 6 December 2017

Available online 13 December 2017

0925-9635/ © 2017 The Authors. Published by Elsevier B.V. This is an open access article under the CC BY license (<http://creativecommons.org/licenses/by/4.0/>).

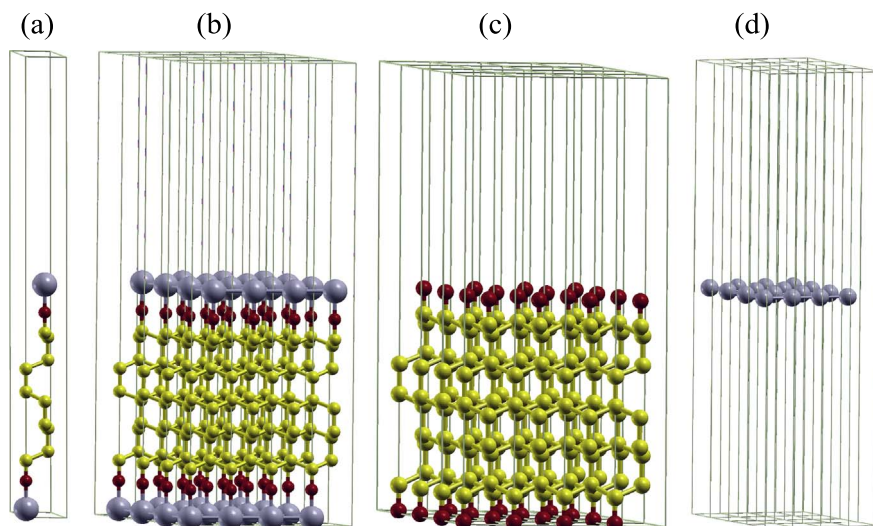


Fig. 1. Interface models: (a) unit cell of slab, (b) $4 \times 4 \times 1$ super cells of slab, (c) parent surface (with terminations), and (d) metallic electrode layer. The large gray, small red, and small yellow balls correspond to the metal, terminating atoms (hydrogen or oxygen), and carbon atoms, respectively. (For interpretation of the references to color in this figure legend, the reader is referred to the web version of this article.)

Cr/Au, can be a better alternative to Ti/Pt/Au [20].

Based on the interest in the electrodes, a number of theoretical works have also studied the adhesion between diamond surfaces and several metals [21–31], but their exploration space has been limited and hence there are still other possibilities of discovering more appropriate electrode metals for diamond surfaces. Pickett and Erwin [21,23] have investigated, for the first time, metal/diamond interfaces for electronic device applications using first-principles local-density functional approaches, inspired by the pioneering work on BN/diamond interfaces by Lambrecht and Segall [22]. They modeled nickel/diamond interfaces on both the (100) and (111) ideal surfaces and computed their Schottky barrier heights and interface energies. It was found that the tetrahedral arrangement leads to an Ohmic interface with the interface energy of 0.97 eV per carbon atom, which suggests that the interface geometry plays a crucial role in its surface electronic structure. Afterward, the Ohmic properties were verified by an experimental work [32] to support the above theory-driven prediction.

Recent works [28–31] examined material structure model and studied several metals. Guo et al. [28] treated 3 metals (Al, Cu, Ti) on clean diamond (111)–(1×1) surface. Monachon et al. [31] treated 2 metals (Cu, Ni) on clean and hydrogen terminated diamond (111)–(1×1) surfaces. These two works evaluated the adhesion strengths by calculating work of separation (W_{sep}), which represents the adhesion strengths between the metals and diamond surfaces. While they treated the model of metallic electrodes as multi-layers of the metals, Motochi et al. [29] modeled the interfaces as periodic slabs comprised of monolayer metallic electrodes and diamond slab with/without monolayer atomic terminations. They applied density functional theory (DFT) approaches to evaluate adsorption energy, E_{ads} , and density of states (DOS) for their target systems. (E_{ads} is notated as the surface cohesive energy, E_{coh} , in their work.) They concluded that tantalum and vanadium were the best metallic electrodes because they showed highest E_{ads} with surface metallic properties, *i.e.* no bandgaps.

In this study, we improved mainly the previous work by Motochi et al. [29] in terms of the following three points: First, although their work gave a great insight into the possibility of the carbide forming metals to form better electrodes, the number of metal samples was quite limited. In contrast, the present study has systematically explored 20 kinds of metals for more desirable diamond electrodes. Second, we adopted the metal/diamond structure model similar to the work by Motochi et al. [29], but we paid more careful attention to the evaluation of adhesion for which we employed W_{sep} instead of E_{ads} from the reason discussed in Section 2. Third, while they discussed only Ohmic contacts, we evaluated Schottky contacts, too.

For pristine surface, our calculations confirmed that Ti has the best

Ohmic contact, which agrees with the fact that Ti is typically used for realizing Ohmic contact [16–20]. We further established that Cr has higher adhesion strength than Ta and V, which were previously reported to have highest adhesion strengths [29]. In contrast, for the oxygenated surface, it is found that (1) Ni has the best Schottky contact and (2) Ti and Cr have highest adhesion strengths with good Schottky contacts.

It is important to note that, while the computational works including ours have studied non-doped diamond, the doping of boron or phosphorus significantly affects the electrode adhesion: It was reported that boron doping reduces the contact resistance of Ti electrode [17]. The work by Teraji et al. confirmed that this tendency is more pronounced with higher doping density for Au and Cu electrodes [33]. The same tendency was also observed for phosphorus doping. Kato et al. showed that heavy phosphorus doping results in an Ohmic contact of the Ti electrode [13], and the contact resistance becomes lower, when the dopant concentration becomes higher.

In this section, we have reviewed previous studies on the diamond surfaces and made a brief explanation of our findings. The following sections are organized as follows: Section 2 presents the surface models and methodology. In Section 3, the results of the work are presented and finally the conclusions drawn from the findings are given in Section 4.

2. Model and methodology

Fig. 1 shows our slab model of interfaces between metallic electrodes and diamond surfaces. Although this figure explains the model with $4 \times 4 \times 1$ super cell for the reader's convenience, all the calculations were conducted with a unit cell. We employed diamond (111) surface as well as the recent theoretical works [29,34] because of its potential applicability for excellent n-type semiconductor, due to the establishment of high phosphorus doping density for the surface. We considered hydrogen and oxygen terminations for the diamond surface following the work by Motochi et al. [29]. Hydrogenated diamond is reported to have high carrier mobility [35] and vigorously applied to metal oxide semiconductor field effect (MOSFET) transistors [36,37]. The surface terminations by oxides are known as not only accelerating carrier mobility [35] but also improving adhesion strengths of transition metal electrodes [29]. We employed the 20 metals, Mg, Al, Ti, V, Cr, Ni, Cu, Zn, Zr, Nb, Mo, Pd, Ag, In, Hf, Ta, W, Pt, Au, and Pb with the three kinds of terminations, which leads in total 60 interface systems that were considered to explore desirable electrodes for power device applications in total. We have performed DFT calculations with carefully chosen computational conditions as explained later in this section

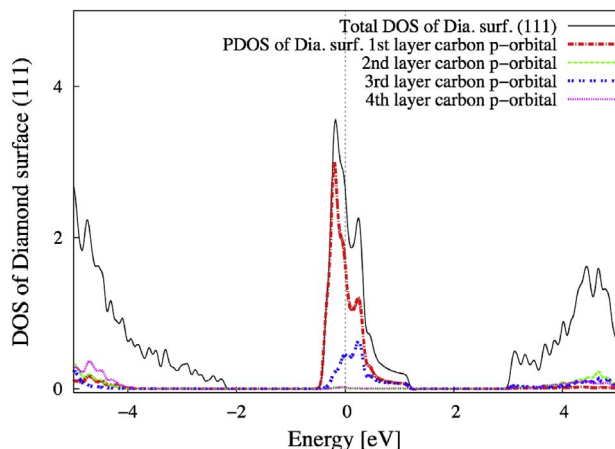


Fig. 2. Partial contributions to DOS from each layer of the diamond slab. Only the first three layers contribute mainly to the surface state appearing between the bulk gap. Energy as the horizontal axis is set with the Fermi energy at 0 eV.

and optimized the geometries using QUANTUM ESPRESSO [38] with PBE-GGA [39] exchange-correlation functional and ultrasoft pseudopotentials [40] available therein.

Most of the preceding works have taken W_{sep} as the measure of adhesion strength [24–26,28,31], which does not include the cohesive energies of the metallic sheets, different from E_{ads} [29]. We have verified whether or not our model can accurately simulate the interfaces in terms of partial density of states (pDOS) at each of the diamond layers, which was not investigated in the previous study [29].

The expression for the work of separation is given by Eq. (1): [28]

$$W_{\text{sep}}(x) = \frac{1}{2\Omega} (E_{\text{parent_surface}} + 2 \cdot E_{\text{sheet}}(x) - E_{\text{slab}}(x)). \quad (1)$$

Here, Ω is the surface area of unit cell, (i) $E_{\text{parent_surface}}$ is the energy per unit cell of the diamond slab with/without termination (parent surface), (ii) $E_{\text{slab}}(x)$ is the energy of the whole interface system (slab) with the sheets of metal x , and (iii) $E_{\text{sheet}}(x)$ is the energy of the sheet of metal x (electrode). The factor 1/2 in Eq. (1) comes from the fact that our slab model has interfaces on both sides. On the other hand, in the case of the adsorption energy [29], $E_{\text{sheet}}(x)$ is replaced by the cohesive energy of the surface atoms from W_{sep} , which brings improper energy gains for the evaluation of adhesion strengths.

Within the framework of the DFT approaches, all the three energies (i), (ii), and (iii) were computed under the conditions that $E_{\text{ecut}}^{\text{wfc}} = 90$ Ry for the cutoff energy of the orbital function expansion and $E_{\text{ecut}}^{\text{rho}} = 520$ Ry to compensate for charges in the ultrasoft pseudopotential evaluation. The k -mesh size (discretization of Brillouin zone) of $14 \times 14 \times 1$ was used for all the three energies. The Marzari-Vanderbilt smearing scheme [41] with $\delta E = 0.02$ Ry was applied to all the systems. The above computational specifications were the best choices for all the systems, but they were also very carefully chosen such that all the evaluations of interface energy lie within the chemical accuracy of ~ 2 mRy/unit cell. Hereafter, we describe how to model the metal-(terminating atom)-diamond interface system (slab) and its subsystems (parent surface and metal) in order to evaluate the corresponding three energies in more detail.

First, we extracted a ten-layer diamond slab with an ideal (111)–(1 × 1) surface from the bulk structure. As confirmed later in Section 3.1, the number of layers is large enough to capture the change in the electronic structure from surface to bulk. To construct the diamond surface, we chose a vacuum phase with dimension of 9.2 Å subject to the periodic boundary condition (Fig. 1), which means that

the upper and lower five layers are identical. In order to take into account surface reconstructions, we optimized both the atomic positions and lattice parameters (*i.e.*, unit cell size) simultaneously within the PBE-GGA method under the above condition. Our optimized geometries reasonably agree with the experiment [42] as well as that by Motochi et al. [29]. The number of the layers (Fig. 1) has been found to be large enough to simulate the (111)–(1 × 1) surfaces because the geometry at the fifth layers from both sides is almost same as that of the bulk. The optimized geometry was used to evaluate $E_{\text{parent_surface}}$. Erwin and Pickett [43] pointed out that the dangling bonds of the (111)–(1 × 1) surface are located at on-top sites. In the case of H- and O-terminations, therefore, we placed the terminating atoms at an on-top site of the above optimized (111)–(1 × 1) surface. Starting with initial atomic configurations separated by their covalent radii [44], we fixed the lattice parameters and reoptimized all the atomic positions and found that both the hydrogen and oxygen terminating atoms stay at the on-top site with only a change in the vertical distance between the surface carbon atom and the terminating atoms.

Secondly, since the on-top site may be thought of as being the most preferable to electrode adhesion, we constructed the slab model by putting metallic monolayers at the on-top site of the optimized (111)–(1 × 1) surface. Starting with initial atomic configurations separated by their covalent radii, we fixed the lattice parameters and reoptimized all the atomic positions to get $E_{\text{slab}}(x)$. Note that our unit cell contains only one metallic atom on the surface. This means that we ignore lattice mismatches at interfaces, but, as discussed in Section 3.4, their influences for W_{sep} were found to be negligible. Similar to the non-termination case, we placed metallic monolayers on the H- or O-terminating diamond surfaces and reoptimized the geometries.

Lastly, we considered the metallic monolayers (*i.e.*, two dimensional metallic sheets) without optimizing their geometries, which was used to evaluate $E_{\text{sheet}}(x)$. The errors due to omitting the optimizations are found to be negligible as discussed later in Section 3.4. Since all the slab systems are non-magnetic, we treated all the 2D sheets as being paramagnetic, irrespective of their actual magnetic states [45].

3. Results and discussion

3.1. Number of diamond layers and metal layers

In order to check whether the number of diamond layers is large enough to simulate the interfaces, we looked into pDOS contributions at each diamond layer to the total DOS, as shown in Fig. 2. We found that $2p$ orbitals from the first three layers mainly contribute to the surface state appearing within the bulk gap. This corresponds to the fact that any surface reconstruction occurs only within the first two layers. This is consistent with previous studies by Pickett and Erwin [23,46]. We note in Fig. 2 that the width of the in-gap peak, ~ 2 eV, is a bit wider than that usually expected for the surface state [47]. We also checked the convergence of W_{sep} with increasing number of metal layers from one to three. Here, we chose Ni electrode on pristine diamond surface as a sample. We assumed the bulk structure for three layers of Ni, since it is difficult to determine the proper structure around the interface. The difference of the adhesion strengths is only 7% between one and three metallic layers, where the values of W_{sep} for the two cases are 5.20 J/m² and 5.63 J/m² respectively. Therefore, we modeled the electrodes with a single layer metal sheet.

3.2. Density of states

The DOS provides us with the useful insights for the electric properties of the interface systems: The DOS of diamond slab has a peak at

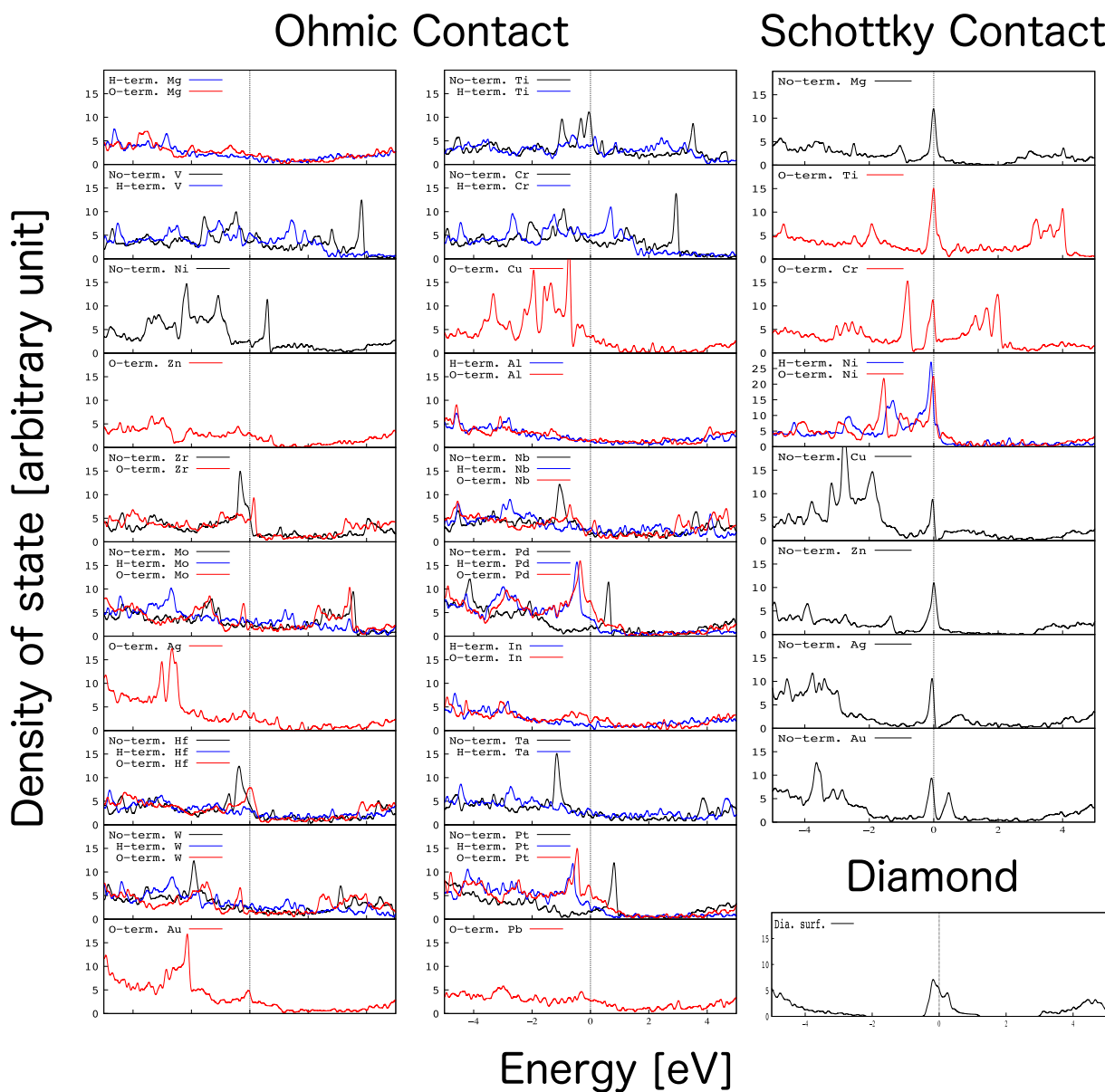


Fig. 3. DOS of the parent surface and the metal sheets with Hydrogen, Oxygen, and no-terminations. Blue, red, and black lines correspond to Hydrogen, Oxygen, and no-terminations respectively. The vertical dotted line represents Fermi energy. The DOS are classified into Ohmic and Schottky contacts respectively. (For interpretation of the references to color in this figure legend, the reader is referred to the web version of this article.)

Fermi energy, E_F . This in-gap peak corresponds to the localized surface electronic state because such a peak is not observed in bulk diamond. For interface systems, the appearance of the peak means the existence of localized electronic state around the interface. It is considered that such localized electronic states appear with the electrode having low carrier mobility across the interface. Since these electronic states give rise to electric double layers that are the origin of electric rectification, in-gap peaks can be regarded as the sign of a Schottky contact, otherwise the electric contact nature is Ohmic. Fig. 3 shows the combinations of electrode metals and surface terminations (no-term., H-term., and O-term.), separating them into Ohmic and Schottky contacts respectively. Another important observation is the DOS at E_F . For Ohmic contact, DOS at E_F corresponds to the density of conduction electrons, while for

Schottky contact, it determines how well electric double layers are formed. On the other hand, higher DOS at E_F is more preferred for both contact types. On the contrary, tiny DOS at Fermi energy means that the conductivity is significantly low. The DOS of such cases are shown in Appendix A. According to this analysis, it is concluded that Ti on the pristine surface is especially good for Ohmic electrode, while Ni on Oxygen or Hydrogen termination excellently realizes Schottky contact.

3.3. Bonding natures and adhesion lengths

Fig. 4 shows the change in the bonding lengths during the lattice relaxation starting off with the initial value taken as the sum of covalent radii of the atoms constituting the interface. There is a clear contrast

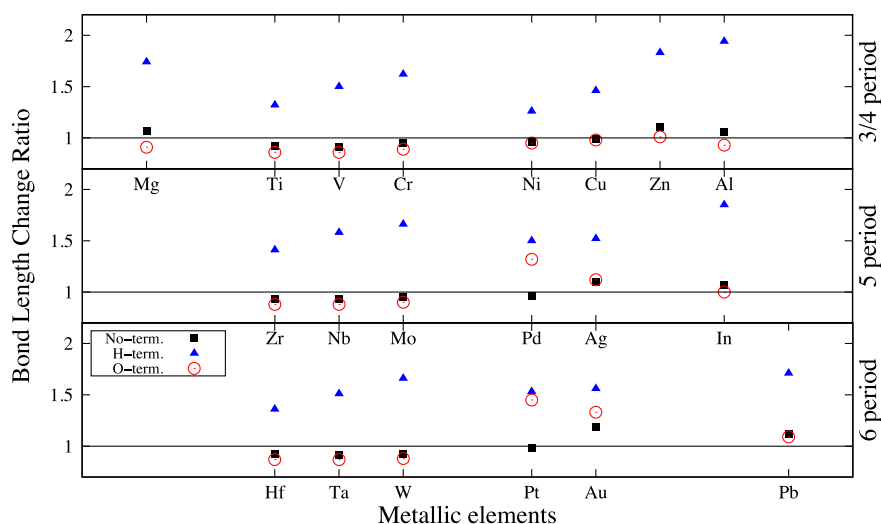


Fig. 4. Deviations of the adhesion lengths, d_{adh} , from the initial values for the geometrical optimizations. The sum of the initial covalent radii is shown to be unity. Open circles (closed triangles) correspond to the lengths between the termination elements and metallic elements (surface carbon atoms). No-term. stands for no-termination while H-term. and O-term. stand for hydrogen- and oxygen-terminated surfaces respectively.

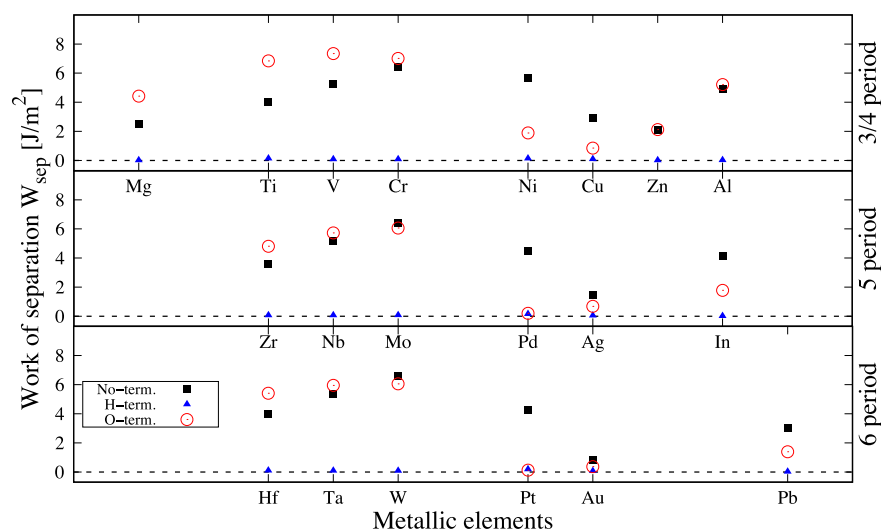


Fig. 5. Work of separation W_{sep} obtained from our PBE-GGA simulations with the ultrasoft pseudopotentials. No-term. stands for no-termination while H-term. and O-term. stand for hydrogen- and oxygen-terminated surfaces respectively.

between elongation or contraction of the adhesion lengths, d_{adh} , after optimization between the initial and optimized bond lengths (atomic positions were optimized from their initial ones separated by the covalent radii of atoms constituting the interfaces, as explained in Section 2). The contrast might be attributed to the different bonding nature, such as ionic or covalent. In the case of no-termination, for instance, Al (Ti) results in elongation (contraction) which is consistent with the covalent (ionic) nature of the elements. Significant elongations for the hydrogen terminations compared with the oxygen terminations and no-terminations might also be attributed to the fact that the diamond surface has only one dangling bond that hybridizes with the hydrogen 1s orbital and then there is no room for additional bonding with the electrode metals. In the case of O-termination, The d_{adh} became shorter [longer] for transition metals (Ti, Ta, V) [noble ones (Au, Pd)]. This contrast can be attributed to whether or not the d/f orbitals of the valence shell are closed, *i.e.*, the noble metals has closed shells, while the transition metals possess open ones.¹ The trend in the magnitude of the contraction can be explained to some extent in terms of the electronegativity: the pronounced contraction by the elements with

the smaller numbering of groups (*i.e.*, left hand side in the periodic table) would be accounted for by the smaller electronegativities. The difference of the negativities between the metallic elements and the top-most atom on the surface (carbon or oxygen) gets larger when the negativity of the metallic element itself gets smaller. The larger difference leads to the ionic bonding nature, and hence to the more pronounced contraction. The scenario is consistent with the fact that we get more contractions by O-termination than no-termination because oxygen has the larger electronegativity and hence gives a larger difference of electronegativity.

3.4. Work of separation

Fig. 5 highlights the dependence of $W_{sep}(x)$ on the metallic elements x and the terminations (*i.e.* no-termination, O- and H-terminations), evaluated from our PBE-GGA simulations with the ultrasoft pseudopotentials. It is found that the overall trend of $W_{sep}(x)$ strongly depends on the termination elements, reflecting their surface bonding natures. In the case of the no-termination the Au electrode has the weakest adhesion as expected. Surprisingly, the Pd electrode is found to have a slightly stronger adhesion than Ti, a carbide forming metal. The group-6 (Cr, Mo and W) basically have stronger adhesion than the other groups. For any metal, the H-termination hinders the metal from forming the electrodes because of no dangling bonds on the surface (see

¹ For Au, the partially occupied 6s orbital can contribute to the bonding with oxygen atoms. However, it may be weak because s orbital has a spherical shape and may have less overlap with p orbital of oxygen than d/f orbitals.

Table 1

Comparison of W_{sep} (J/m^2) between our values and the previous theoretical works using DFT (density functional theory) for several metals (Al, Cu, Ti, and Ni). The corresponding adhesion lengths, d_{adh} , are also given in parentheses. Note that the present metal/diamond interface models employ monolayer metallic sheets, while the previous ones did multi-layer metallic sheets.

	This work	H. Guo et al. [28]	C. Monachon et al. [31]	Y. Qi and L.G. Hector [26]
Al	4.90 J/m^2 (2.09 Å)	4.08 J/m^2 (1.86 Å)	N/A	3.98 J/m^2 (1.86 Å)
Cu	2.90 J/m^2 (2.06 Å)	3.36 J/m^2 (2.09 Å)	3.04 J/m^2 (N/A)	N/A
Ti	4.04 J/m^2 (2.18 Å)	5.77 J/m^2 (1.94 Å)	N/A	N/A
Ni	5.65 J/m^2 (1.92 Å)	N/A	5.00 J/m^2 (1.96 Å)	N/A

Section 3.3). In contrast, the O-termination results in quite different effects on the adhesion. While it weakens the adhesion of the noble metals (Pt, Au, Ag, Pd, and Cu), it strengthens that of some transition metals (group-4,5,6), especially Ti and V. The combination of Ti and pristine diamond surface has both fairly high adhesion strength and the best Ohmic contact, which is consistent with the fact that Ti is a typically used metal to realize Ohmic contact [16–20]. It is also reproduced that the combinations of Ta and V with pristine diamond surface have highest adhesion strengths with good Ohmic contacts [29]. In addition, it is established that Cr on pristine diamond surface had a slightly higher adhesion strength. While Ni on oxygenated and hydrogenated diamond surfaces show the best Schottky contacts, their adhesion strengths are rather weak. On the other hand, Ti and Cr on oxygenated diamond surfaces show good Schottky contacts with the best adhesion strengths.

Table 1 compares our numerical results of W_{sep} and d_{adh} with those by previous studies [26,28,31] for Ni, Cu, Al, and Ti. Note that our metal/diamond interface models consider only monolayers, while the previous ones adopt multi-layers. Despite such a difference, we found that our numerical results for Cu and Ni agree well with the previous ones (their differences in W_{sep} and d_{adh} lie within $\sim 0.6 \text{ J}/\text{m}^2$ and $\sim 0.04 \text{ Å}$, respectively). On the other hand, our results overestimate d_{adh} for Al and Ti. Interestingly, the overestimation affects W_{sep} in the opposite manner, *i.e.*, W_{sep} increases (decreases) for Al (Ti). This may be explained by the different nature of the bonding, *i.e.*, covalent for Al and ionic for Ti as discussed in Section 3.3: Covalent bonds generally tend to have longer bond lengths (*e.g.*, sparse structure in diamond structure) than ionic ones (*e.g.*, NaCl structure). The optimal d_{adh} for Al would be longer than the previous ones and closer to ours, leading to a stronger adhesion. On the other hand, our predicted d_{adh} for Ti seems to deviate from the optimal one, leading to a weaker adhesion.

We note that the present work did not take explicitly into account the energy loss/gain by the lattice relaxation. The metallic ion is located just above the carbon atom in our slab model. This corresponds to that the lattice of metallic sheet is forced to have the same lattice

Appendix A

In Fig. 6, we present the DOS for the combinations of metals and surface states which are neither Ohmic nor Schottky in the sense that tiny DOS exist at the Fermi energy as mentioned in Section 3.2.

constant as the diamond surface. We may estimate the energy loss due to this artificial distortion. From the values of bulk modulus of metals obtained in literature, we can roughly estimate the energy loss that arises when the lattice of metallic sheets is distorted towards that of diamond surface. Taking Birch-Murnaghan equation of state [48], we estimate the loss being 0.377 J/m^2 for Au, 0.015 J/m^2 for Pd, 0.073 J/m^2 for Ti, 0.342 J/m^2 for V, and 0.078 J/m^2 for Ta. Such energy losses are negligibly small compared with $W_{\text{sep}}(x)$ of the metal sheets that show good adhesion.

4. Conclusion

We have confirmed that Ti with pristine diamond surface has the best Ohmic contact, which is consistent with the previous investigations [16–20], and established the combination of Cr and pristine diamond surface has higher adhesion strength than those of Ta or V and pristine diamond surface, which was reported previously to have highest adhesion strength [29]. While Ni on oxygenated and hydrogenated diamond surfaces show the best Schottky contacts, their adhesion strengths are rather weak. On the other hand, Ti and Cr on oxygenated diamond surface show the highest adhesion strengths, with good Schottky contact. It is established that metal layers can hardly attach to hydrogenated diamond surface, because there is no dangling bond from hydrogen towards the metal. It is also observed that oxygenated surface weakens the adhesion strengths and increases the adhesion lengths, d_{adh} , for noble metals (Pt, Au, and Pd), which implies d valence orbitals (*e.g.* d_{z^2}) are necessary for the metals to bond with surface oxygens. For the other cases, it is found that the adhesion lengths correlate weakly and negatively with the strength of bonding ionic nature.

Acknowledgments

The computations in this work have been performed using the facilities of the Center for Information Science in JAIST. This work was supported by the Kenya National Council for Science and Technology (NCST, Now National Commission for Science, Technology and Innovation (NACOSTI)) Grant No. NCST/5/003/4th CALL/050, and the Computational Materials Sciences Group, Department of Physics, University of Eldoret, Kenya. Authors, IM, NWM, and GOA wish to acknowledge the Center for High Performance Computing (CHPC) in Cape Town South Africa for computational resources. KH is grateful for financial support from a KAKENHI grant (15K21023,17K17762), a Grant-in-Aid for Scientific Research on Innovative Areas (16H06439),PRESTO (JPMJPR16NA) and the “Materials research by Information Integration” Initiative (MI²I) project of the Support Program for Starting Up Innovation Hub from Japan Science and Technology Agency (JST). R.M. is grateful for financial support from TOKUYAMA Science Foundation, MEXT-KAKENHI grants 17H05478, the support by FLAGSHIP2020, MEXT for the computational resources, Project Nos. hp170269 and hp170220 at K-computer.

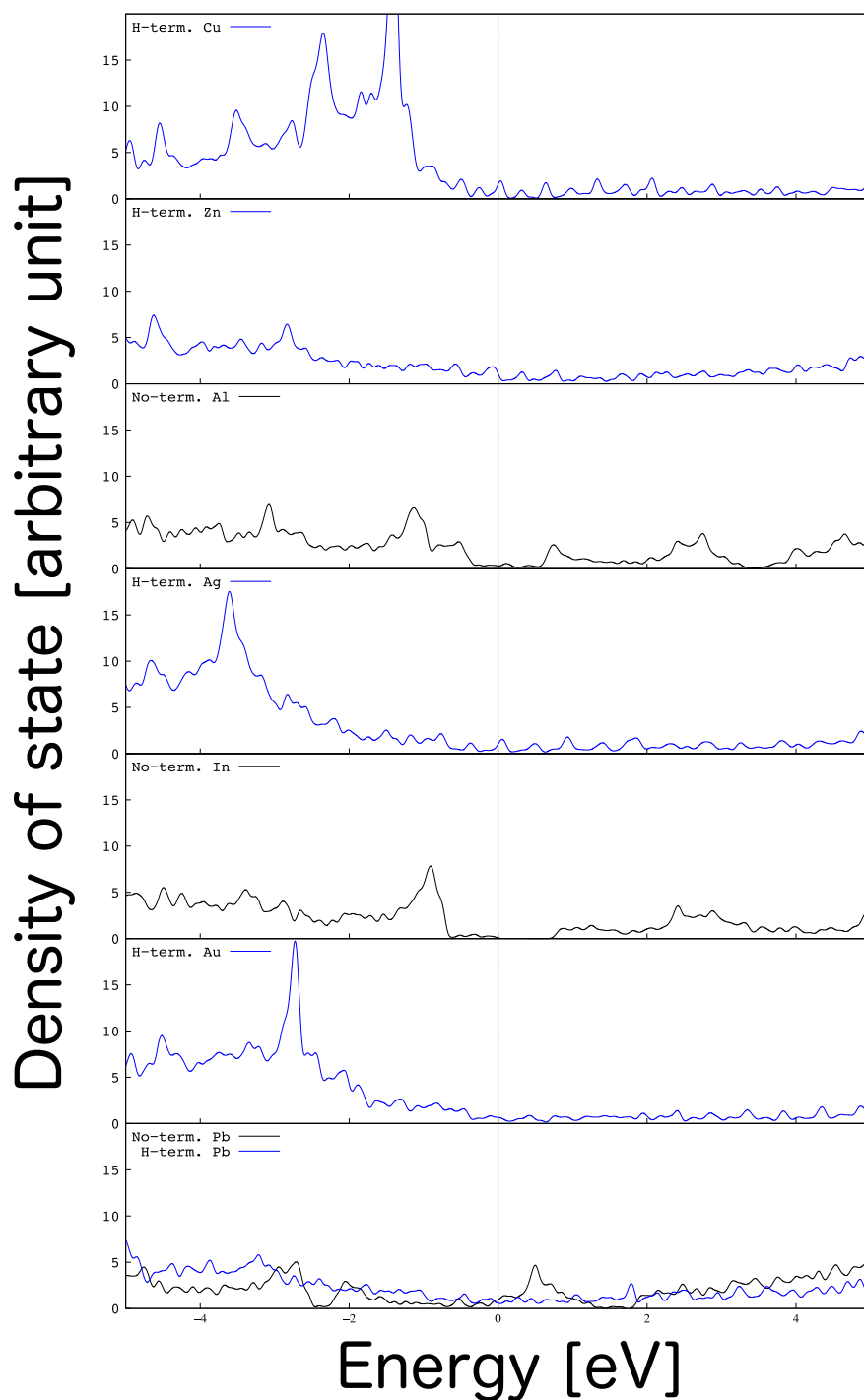


Fig. 6. DOS of the parent surface and the metal sheets with Hydrogen and no-terminations. They all correspond to a bonding configuration that leads to neither Ohmic or Schottky contact. Blue, red, and black lines correspond to Hydrogen, Oxygen, and no-terminations respectively. The vertical dotted line represents the Fermi energy. (For interpretation of the references to color in this figure legend, the reader is referred to the web version of this article.)

References

- [1] R. Maezono, A. Ma, M.D. Towler, R.J. Needs, Equation of state and Raman frequency of diamond from quantum Monte Carlo simulations, *Phys. Rev. Lett.* 98 (2007) 025701.
- [2] M. Willander, M. Friesel, Q. Wahab, B. Straumal, Silicon carbide and diamond for high temperature device applications, *J. Mater. Sci. Mater. Electron.* 17 (2006) 1–25.
- [3] R. Maezono, N.D. Drummond, A. Ma, R.J. Needs, Diamond to β -tin phase transition in Si within diffusion quantum Monte Carlo, *Phys. Rev. B* 82 (2010) 184108.
- [4] J. Achard, F. Silva, A. Tallaire, X. Bonnin, G. Lombardi, K. Hassouni, A. Gicquel, High quality MPACVD diamond single crystal growth: high microwave power density regime, *J. Phys. D: Appl. Phys.* 40 (20) (2007) 6175.
- [5] N. Tsubouchi, A. Chayahara, Y. Mokuno, H. Yamada, Large Single Crystal Diamond Plates Produced by Microwave Plasma CVD, *Silicon Carbide and Related Materials 2008, (2009)*, pp. 991–994.
- [6] H. Yamada, A. Chayahara, Y. Mokuno, N. Tsubouchi, S. Shikata, Uniform growth and repeatable fabrication of inch-sized wafers of a single-crystal diamond, *Diam. Relat. Mater.* 33 (2013) 27–31.
- [7] S. Nad, Y. Gu, J. Asmussen, Growth strategies for large and high quality single crystal diamond substrates, *Diam. Relat. Mater.* 60 (2015) 26–34.
- [8] R. Ramamurti, M. Becker, T. Schuelke, T. Grotjohn, D. Reinhard, J. Asmussen, Deposition of thick boron-doped homoepitaxial single crystal diamond by

- microwave plasma chemical vapor deposition, *Diam. Relat. Mater.* 18 (5) (2009) 704–706 Proceedings of Diamond 2008, the 19th European Conference on Diamond, Diamond-Like Materials, Carbon Nanotubes, Nitrides and Silicon Carbide.
- [9] T. Grotjohn, S. Nicley, D. Tran, D.K. Reinhard, M. Becker, J. Asmussen, Single crystal boron-doped diamond synthesis, *MRS Proc.* 1203 (2009).
- [10] R. Issaoui, J. Achard, A. Tallaire, F. Silva, A. Gicquel, R. Bisaro, B. Servet, G. Garry, J. Barjon, Evaluation of freestanding boron-doped diamond grown by chemical vapour deposition as substrates for vertical power electronic devices, *Appl. Phys. Lett.* 100 (12) (2012) 122109.
- [11] A.L. Vikharev, A.M. Gorbachev, M.A. Lobaev, A.B. Muchnikov, D.B. Radishev, V.A. Isaev, V.V. Chernov, S.A. Bogdanov, M.N. Drozdov, J.E. Butler, Novel microwave plasma-assisted CVD reactor for diamond delta doping, *Phys. Status Solidi RRL* 10 (4) (2016) 324–327.
- [12] J.E. Butler, et al., Nanometric diamond delta doping with boron, *Phys. Status Solidi RRL* 11 (2017) 1600329.
- [13] H. Kato, D. Takeuchi, N. Tokuda, H. Umezawa, H. Okushi, S. Yamasaki, Characterization of specific contact resistance on heavily phosphorus-doped diamond films, *Diam. Relat. Mater.* 18 (5) (2009) 782–785 Proceedings of Diamond 2008, the 19th European Conference on Diamond, Diamond-Like Materials, Carbon Nanotubes, Nitrides and Silicon Carbide.
- [14] T. Grotjohn, D. Tran, M. Yaran, S. Demlow, T. Schuelke, Heavy phosphorus doping by epitaxial growth on the (111) diamond surface, *Diam. Relat. Mater.* 44 (2014) 129–133.
- [15] H. Kato, T. Makino, S. Yamasaki, H. Okushi, n-Type diamond growth by phosphorus doping on (001)-oriented surface, *J. Phys. D: Appl. Phys.* 40 (2007) 6189.
- [16] I. Meyyappan, A. Malshe, H. Naseem, W. Brown, Au/(Ti-W) and Au/Cr metallization of chemically vapor-deposited diamond substrates for multichip module applications, *Thin Solid Films* 253 (1994) 407–412.
- [17] C. Johnston, P. Chalker, I. Buckley-Golder, M. van Rossum, M. Werner, E. Obermeier, High temperature contacts to chemically vapour deposited diamond films — reliability issues, *Mater. Sci. Eng. B* 29 (1995) 206–210 European Materials Research Society 1994 Spring Meeting Symposium E: High Temperature Electronics: Materials, Devices and Applications.
- [18] H. Hoff, G. Waytena, C. Vold, J. Suehle, I. Isaacson, M. Rebbert, D. Ma, K. Harris, Ohmic contacts to semiconducting diamond using a Ti/Pt/Au trilayer metallization scheme, *Diam. Relat. Mater.* 5 (12) (1996) 1450–1456.
- [19] C. Iacovangelo, Thermal stability of metallized CVD diamond, *Thin Solid Films* 286 (1996) 264–269.
- [20] S. Msolli, J. Alexis, H. Kim, Mechanical behavior and adhesion of the Ti/Cr/Au metallization scheme on diamond substrate, *Adv. Eng. Mater.* 19 (2017) 1700109.
- [21] W.E. Pickett, Thin superlattices and band-gap discontinuities: the (110) diamond-boron nitride interface, *Phys. Rev. B* 38 (1988) 1316–1322.
- [22] W.R.L. Lambrecht, B. Segall, Electronic structure of (diamond C)/(sphalerite BN) (110) interfaces and superlattices, *Phys. Rev. B* 40 (1989) 9909–9919.
- [23] S.C. Erwin, W.E. Pickett, Diamond-nickel interfaces: calculation of the electronic and atomic structure and Schottky barriers, *Surf. Coat. Technol.* 47 (1991) 487–495.
- [24] X.-G. Wang, J.R. Smith, Copper/diamond adhesion and hydrogen termination, *Phys. Rev. Lett.* 87 (2001) 186103.
- [25] Y. Qi, L.G. Hector, Hydrogen effect on adhesion and adhesive transfer at aluminum/diamond interfaces, *Phys. Rev. B* 68 (2003) 201403.
- [26] Y. Qi, L.G. Hector, Adhesion and adhesive transfer at aluminum/diamond interfaces: a first-principles study, *Phys. Rev. B* 69 (2004) 235401.
- [27] Y. Jia, W. Zhu, E.G. Wang, Y. Huo, Z. Zhang, Initial stages of Ti growth on diamond (100) surfaces: from single adatom diffusion to quantum wire formation, *Phys. Rev. Lett.* 94 (2005) 086101.
- [28] H. Guo, Y. Qi, X. Li, Adhesion at diamond/metal interfaces: a density functional theory study, *J. Appl. Phys.* 10 (2010).
- [29] I.T. Motochi, N.W. Makau, G.O. Amolo, Metal-semiconductor ohmic contacts: an ab initio Density Functional Theory study of the structural and electronic properties of metal-diamond (111)-(1 × 1) interfaces, *Diam. Relat. Mater.* 23 (2012) 10–17.
- [30] A.K. Tiwari, J.P. Goss, P.R. Briddon, N.G. Wright, A.B. Horsfall, M.J. Rayson, Electronic and structural properties of diamond (001) surfaces terminated by selected transition metals, *Phys. Rev. B* 86 (2012) 155301.
- [31] C. Monachon, G. Schusteritsch, E. Kaxiras, L. Weber, Qualitative link between work of adhesion and thermal conductance of metal/diamond interfaces, *J. Appl. Phys.* 115 (2014).
- [32] J. van der Weide, R.J. Nemanich, Influence of interfacial hydrogen and oxygen on the Schottky barrier height of nickel on (111) and (100) diamond surfaces, *Phys. Rev. B* 49 (1994) 13629–13637.
- [33] T. Teraji, S. Koizumi, H. Kanda, Ohmic contacts for phosphorus-doped n-type diamond, *Phys. Status Solidi A* 181 (1) (2000) 129–139.
- [34] C. Monachon, G. Schusteritsch, E. Kaxiras, L. Weber, Qualitative link between work of adhesion and thermal conductance of metal/diamond interfaces, *J. Appl. Phys.* 115 (12) (2014) 123509.
- [35] M.M. Hassan, K. Larsson, Effect of surface termination on diamond (100) surface electrochemistry, *J. Phys. Chem. C* 118 (2014) 22995–23002.
- [36] S. Russell, S. Sharabi, A. Tallaire, D.A.J. Moran, RF operation of hydrogen-terminated diamond field effect transistors: a comparative study, *IEEE Trans. Electron Devices* 62 (2015) 751.
- [37] Hydrogen-terminated diamond vertical-type metal oxide semiconductor field-effect transistors with a trench gate, *Appl. Phys. Lett.* 109 (2016) 033503.
- [38] P. Giannozzi, et al., QUANTUM ESPRESSO: a modular and open-source software project for quantum simulations of materials, *J. Phys. Condens. Matter* 21 (2009) 395502.
- [39] J.P. Perdew, K. Burke, M. Ernzerhof, Generalized gradient approximation made simple, *Phys. Rev. Lett.* 77 (1996) 3865; *Phys. Rev. Lett.* 78 (1997) 1396–1396.
- [40] C.J. Pickard, M.C. Payne, Second-order $k \cdot p$ perturbation theory with Vanderbilt pseudopotentials and plane waves, *Phys. Rev. B* 62 (2000) 4383–4388.
- [41] N. Marzari, D. Vanderbilt, A. De Vita, M.C. Payne, Thermal contraction and disordering of the Al(110) surface, *Phys. Rev. Lett.* 82 (1999) 3296–3299.
- [42] Y. Yan, S.B. Zhang, M.M. Al-Jassim, Graphite-like surface reconstructions on C(111) and their implication for n-type diamond, *Phys. Rev. B* 66 (2002) 201401.
- [43] S.C. Erwin, W.E. Pickett, Diamond-nickel interfaces: calculation of the electronic and atomic structure and Schottky barriers, *Surf. Coat. Technol.* 47 (1991) 487–495.
- [44] B. Cordero, V. Gomez, A.E. Platero-Prats, M. Reves, J. Echeverria, E. Cremades, F. Barragan, S. Alvarez, Covalent radii revisited, *Dalton Trans.* (2008) 2832–2838.
- [45] K. Hongo, R. Maezono, Y. Kawazoe, H. Yasuhara, M.D. Towler, R.J. Needs, Interpretation of Hund's multiplicity rule for the carbon atom, *J. Chem. Phys.* 121 (2004) 7144–7147.
- [46] W.E. Pickett, S.C. Erwin, Electronic structure of an ideal diamond-nickel (001) interface, *Phys. Rev. B* 41 (1990) 9756–9765.
- [47] F.J. Himpsel, D.E. Eastman, P. Heimann, J.F. van der Veen, Surface states on reconstructed diamond (111), *Phys. Rev. B* 24 (1981) 7270–7274.
- [48] F. Birch, Finite elastic strain of cubic crystals, *Phys. Rev.* 71 (1947) 809–824.